ELSEVIER

Journal of Chromatography A, 831 (1999) 149–165

JOURNAL OF CHROMATOGRAPHY A

Flow distribution in chromatographic columns[1]

Q.S. Yuan, A. Rosenfeld, T.W. Root, D.J. Klingenberg, E.N. Lightfoot*

Department of Chemical Engineering, University of Wisconsin–Madison, 1415 Engineering Drive, Madison, WI 53706, USA

Received 2 July 1998; received in revised form 10 October 1998; accepted 27 October 1998

Abstract

It becomes increasingly clear that flow non-uniformity frequently limits the performance of chromatographic columns, and that there are at least two major causes for this: non-uniform packing and inadequate header design. Static magnetic resonance imaging (MRI) of small columns in this laboratory has confirmed previous reports of packing non-uniformity and found void fractions to be smallest in the neighborhood of the wall while the central and upstream regions of the column are more loosely packed. Both static and flow MRI suggests that additional mal-distribution is introduced by non-uniform flow in headers, especially for short columns. Flow non-uniformity can reduce resolution directly, and it can also limit column capacity through perturbation-induced viscous fingering. A preliminary stress–strain analysis during column packing is reported which shows that the stress distribution depends strongly upon column aspect ratio (length/diameter) and is most favorable for low values. At the same time adequate flow distribution becomes more difficult as this ratio decreases, and this requires careful attention to the column headers. We therefore suggest a new strategy for header design and provide two specific examples which produce very nearly uniform residence time for all streamlines as well as uniform exit velocity.

Keywords: Magnetic resonance imaging; Packing uniformity; Flow distribution; Column packing

1. Introduction

Currently available models for separation prediction and column scale-up are only valid in the one-dimensional limit where flow is unidirectional and radially uniform. However, in reality, flow distributions in chromatographic columns have been known to be non-uniform for decades [1–6]. Recent magnetic resonance imaging (MRI) [7–11] showed that protein bands are often severely distorted, causing extra peak broadening and asymmetry at the outlet. To make matters worse, the viscosity differences between protein bands and eluting buffers tend to amplify such distortions [8], turning what are initially small disturbances of protein bands into large ''fingers'', thus further decreasing column efficiencies. Therefore, it is desirable to eliminate the onset of any small disturbances in the column and its headers. The two well-known sources for such disturbances are inhomogeneous packing and non-uniform header flow. In this study, we follow the basic physics in transport phenomena to address these two issues separately. We begin by initiating an

*Corresponding author. Tel.: +1-608-262-1092, Fax: +1-608-262-5434, E-mail: enlight@engr.wisc.edu

[1]Presented at the 1998 International Symposium on Preparative Chromatography, Ion Exchange and Adsorption/Desorption Processes and Related Techniques, Washington, DC, 31 May–3 June 1998.

0021-9673/99/$ – see front matter
PII: S0021-9673(98)00924-8

analysis of stress and deformation in granular beds and show that a relatively simple analysis of small stresses can provide useful insight. We then present a new header design principle and provide two examples which produce very nearly uniform residence times and exit velocities for all fluid streamlines.

2. Column packing

2.1. Background and theory

Early studies of packing inhomogeneity focused on the so-called ''wall effects'', where velocity and dispersion were found to be higher near the wall for dry packed columns. Further more, the wall region could extend as far as 30 particle diameters into the column [2–4]. Consequently, ''infinite diameter'' columns were proposed where an injection made at the center of the inlet can traverse the entire length of the column without ever dispersing into the wall region [12]. However, high costs of solvents, media and columns make such designs uneconomic, and they are seldom if ever used.

More recently Farkas and co-workers [13–16] performed detailed experiments to determine the distributions of the local values of the mobile phase velocity, axial dispersion and solute concentration. Their dispersion results agree qualitatively with the early studies but found velocity to be higher at the center than at the wall. They attributed this discrepancy with the earlier findings to the wet packing methods used in their studies. Today almost all columns are wet packed. In our laboratory, static MRI of packing density in a series of small prepacked columns [17] revealed packing densities to be higher near the column exit and the wall than in the upper and central regions, qualitatively in agreement with the velocity profile measured by Farkas et al. This is a critical fact since radial variations have a far more serious effect on column performance than axial variations [17].

The improvement of column packing is hindered by a lack of understanding of the physics which governs the packing process, and it is our purpose here to begin an examination which is based firmly upon known principles. Column packing is essentially a process of pressure filtration of a concentrated slurry, and it can be accomplished by a variety of means [18]. We model all such processes as the interaction of two co-existing pseudo-continuous ''phases'': the assembly of packing particles and the percolating fluids. Since the packing particles of modern columns settle slowly in suspension, we can concentrate our attention on the condensed region of the forming bed. Because motions of both particles and fluid in these condensed regions are slow, we can also neglect inertial forces for both phases.

We begin by writing a momentum balance for the particle phase, which is just a specialized form of a force balance under the assumed conditions:

$$[\nabla \cdot \boldsymbol{\sigma}] = \left(\frac{1-\phi}{\phi}\right)\nabla P - \rho_s \mathbf{g} \tag{1}$$

Here $\boldsymbol{\sigma}$ is the stress matrix of the solid phase; ϕ is the local fraction of column volume occupied by the solid particles ($\phi = 1-\epsilon$, where ϵ is the local interstitial void fraction); P is the fluid pressure; ρ_s is the density of the packing material; and $\mathbf{g}$ is the gravitational force per unit mass. The terms on the right-hand side are body forces acting on the solid phase which are caused by fluid drag and gravity, and they balance the solid phase stress on the left-hand side. In most cases of interest to us, the fluid drag force dominates.

The pressure gradient can be determined from Darcy's law:

$$\mathbf{w} - \mathbf{u} = -\frac{\kappa}{(1-\phi)}\nabla P \tag{2}$$

where $\mathbf{w}$ and $\mathbf{u}$ are the locally averaged observable fluid and solid velocities, respectively; κ is the local permeability of the packed bed, and can be derived from the Blake–Kozeny equation [19]:

$$\kappa = \frac{d_p^2}{150\mu_f} \cdot \frac{(1-\phi)^3}{\phi^2} \tag{3}$$

where μ_f is the dynamic fluid viscosity, and d_p is the diameter of the particles, assumed spherical. It remains to find a constitutive relation to relate stress and motion for the particulate phase and to select a useful set of boundary conditions.

The one-dimensional sedimentation process has received extensive studies [20–24], and for it one need only consider the compressive stress σ_{zz}. Much

of the theory in this case has been based on the work of Kynch [20], who described the behavior of the freely settling suspension by the conservation equation for the particles,

$$\frac{\partial \phi}{\partial t} + \frac{\partial [\phi u(\phi)]}{\partial \phi} \cdot \frac{\partial \phi}{\partial z} = 0 \tag{4}$$

The solution to this partial differential equation depends on the flux curve $\phi u(\phi)$ vs. ϕ, as well as the initial spatial distribution of the particles. Rhee et al. [25], summarized the results of many earlier efforts to solve the one-dimensional problem based on Kynch's theory.

In chromatographic processes, radial variation are far more important than axial variation. Therefore one must consider both shear and compressive stresses, and the resulting two- or three-dimensional motion. This situation has recently been examined by Östergren et al. [26], where these workers considered elastic behavior and made macroscopic measurements.

We begin a study of density distribution for axi-symmetric conditions in a cylindrical packed column by considering both axial and radial variations, and our first problem is to select a constitutive equation for relating stress and deformation of the packing. There is relatively little quantitative information available, but we can make some useful qualitative observations based on the behavior of deformable solids in general. Most importantly, consolidated granular beds normally exhibit reversible elastic deformation until some critical yield point is reached where irreversible plastic flow begins [27]. A number of plasticity theories regarding yield point have been proposed for granular materials under three dimensional stresses. For our axi-symmetric situation, they are of the following form:

$$\begin{aligned} f(\boldsymbol{\sigma}_{ij}) = {} & \boldsymbol{\sigma}_{rr}^2 + \boldsymbol{\sigma}_{\theta\theta}^2 + \boldsymbol{\sigma}_{zz}^2 \\ & + (2 - A)(\boldsymbol{\sigma}_{rr}\boldsymbol{\sigma}_{\theta\theta} + \boldsymbol{\sigma}_{zz}\boldsymbol{\sigma}_{rr} + \boldsymbol{\sigma}_{zz}\boldsymbol{\sigma}_{\theta\theta}) \\ & + A\boldsymbol{\sigma}_{rz}^2 = \boldsymbol{\sigma}_{\text{crit}}^2 \end{aligned} \tag{5}$$

where A is a function of void fraction. When $A = 3$, Eq. (5) reduces to the famous von Mises yield criterion in solid mechanics.

In this paper, we examine the linear elastic limit in which the stress–strain relationship is given by

$$\boldsymbol{\sigma} = 2\mu \mathbf{e} + \lambda e_v \boldsymbol{\delta} \tag{6}$$

where $\mathbf{e}$ is the strain matrix, of which e_v is the trace; $\boldsymbol{\delta}$ is the Kronecker delta, and μ and λ are the Lamé constants. Further more, $\mathbf{e}$ is related to displacement vector ($\mathbf{s}$) through the following equation:

$$\mathbf{e} = \frac{1}{2}\left[\nabla \mathbf{s} + (\nabla \mathbf{s})^T\right] \tag{7}$$

Substituting Eqs. (2), (6), (7) into Eq. (1) and letting u be zero for steady-state, we arrive at:

$$\mu \nabla^2 \mathbf{s} + (\lambda + \mu)\nabla(\nabla \cdot \mathbf{s}) = -\frac{150\mu_f}{d_p^2} \cdot \left(\frac{\phi}{1-\phi}\right)^2 \mathbf{w} - \rho_s \mathbf{g} \tag{8}$$

This is the steady-state form of the Navier equation for linear elastic solids. The boundary conditions we consider are:

$$(1)\ \text{at } z = 0,\ s_z = s_r = 0 \tag{9}$$

$$(2)\ \text{at } z = L,\ \boldsymbol{\sigma}_{zz} = \boldsymbol{\sigma}_{rz} = 0 \tag{10}$$

$$(3)\ \text{at } r = 0,\ \frac{\partial s_r}{\partial r} = \frac{\partial s_z}{\partial z} = 0 \tag{11}$$

$$(4)\ \text{at } r = R,\ s_r = 0,\ \boldsymbol{\sigma}_{rz} = C_w + \mu_w \boldsymbol{\sigma}_{rr} \tag{12}$$

where μ_w is the wall friction coefficient, C_w is the adhesion at the wall. In practice, wall friction as described by Eq. (12) is important, and Östergren et al. have actually determined friction coefficient (μ_w) for one commercial packing. Here however, we shall consider the limiting case of the no slip wall, where μ_w is infinite, and thus $s_z = s_r = 0$ at the wall.

2.2. Results and discussion

Solutions to Eqs. (8)–(12) using a finite difference method are presented for column aspect ratios (L/D) of 5, 1 and 0.5. For the solid phase, parameters for silica are used such that $\mu = 3.2 \cdot 10^{10}$ Pa, $\lambda = 1.5 \cdot 10^{10}$ Pa, and $\rho_s = 2.2 \cdot 10^3$ kg/m^3. The total body force (right hand side of Eq. (8)) is assumed constant and equal to $10 \cdot \rho_s g$; the absolute number has no effect on the shape of the stress distribution curves.

The local axial and radial displacements are calculated by integrating Eq. (8), and the stress distribution calculated according to Eqs. (6) and (7).

Figs. 1–3 are plots of axial displacements in *r*- and *z*-directions for the three columns simulated. For columns with small aspect ratios, Fig. 1 shows that over a large portion of the height of the bed the solid phase has the same axial displacement. This suggests that the friction on the wall is the dominant force which holds up the bed. As the column becomes wider (Figs. 2 and 3), the wall effects gradually diminish towards the center of the column as expected.

The stress distributions as shown in Figs. 4–6 offer more detailed explanations of the column packing structure. The non-zero components of the stress matrix in axi-symmetric cylindrical coordinates are σ_{zz}, σ_{rr}, $\sigma_{\theta\theta}$ and σ_{rz}. Although all four contribute to column packing equally importantly, the effects of σ_{rr} and $\sigma_{\theta\theta}$ are more subtle than those of σ_{zz} (compressive stress) and σ_{rz} (shear stress). Figs. 4 and 5 are contour plots of σ_{zz} and σ_{rz} for all three columns. The parabolic radial variation in compressive stress is in agreement with experimental observations in the powder packing literature [28]. The shear stresses, on the other hand, are the highest around the wall due to wall friction. The combined effects of all stresses are assessed through von Mises yield criteria ($\sqrt{f(\sigma_{ij})}$ in Eq. (5) with $A=3$), and the results are shown in Fig. 6, from which it is clear that plastic deformation will begin around the wall and the bottom of the column. In particulate systems, plastic deformation is caused by particles sliding against each other, and thus causing more compact structure. Therefore, the calculated equivalent stress distribution indicates that the wall region is likely to be more densely packed than the center of the column. This is consistent with our MRI observations as well as the velocity measurement by Farkas et al.

The results in Figs. 4–6 also show that as the column gets wider, the radial variations in all stresses decrease. This is as expected since the effect of the wall will be less felt at the center for wider columns. In fact, when the column is sufficiently wide, there will be a center core where the stresses are radially uniform. This radial uniformity is a desirable feature in a chromatographic column. However, in practice, wide columns are in general more difficult to pack for a variety of reasons. Furthermore, wide columns demand better fluid distribution at the inlet.

We can, however, say very little about the quantitative nature of densification because it must always be accompanied by plastic flow. Further progress must wait on a more realistic constitutive equation which describes both elastic and plastic flows.

3. A new approach to header design

3.1. Background and theory

In a liquid chromatography column, a header is always present to distribute fluid evenly over the cross-section of the column at the feed point and as a collector at the exit. Since most columns operate in essentially reversible Darcy flow, the two headers are normally identical, but, for reasons stated above the inlet header is the more important. The essential part of the conventional distributors involves a variation of either a flat porous disc or a non-penetrable disc with branching channels. Both of these designs create a sudden expansion at the inlet because the plates are flat, but critical quantitative evaluations of performance in terms of the defining equations of motion appear not to exist. Most header designs include a void space above the porous disc to allow rapid radial flow. A search for patents [29–38] revealed more efforts to improve distributor designs in order to achieve uniform flow through distributors but no actual tests or analysis of their performance.

An ideal header must satisfy two criteria: (1) the velocity profile must be flat at the exit of the distributor, and (2) all the streamlines must have identical residence times, thus to guarantee that the protein band or front is flat when it reaches the packed bed. The equations governing the flow inside the header are the continuity equation and the Blake–Kozeny equation (Eq. (2)) for porous media. For an incompressible fluid the continuity equation is

$$\nabla \cdot \mathbf{v} = 0 \tag{13}$$

where $\mathbf{v}$ is the superficial velocity [$\mathbf{v}=(1-\phi)\cdot\mathbf{w}$]. Substituting Eq. (2) with $\mathbf{u}=0$ for the distributor, Eq. (13) becomes

$$\nabla \cdot \kappa \nabla P = 0 \tag{14}$$

with κ defined in Eq. (3). Eq. (14) can be solved for pressure field in a specific header. The velocity profile can then be computed from the pressure

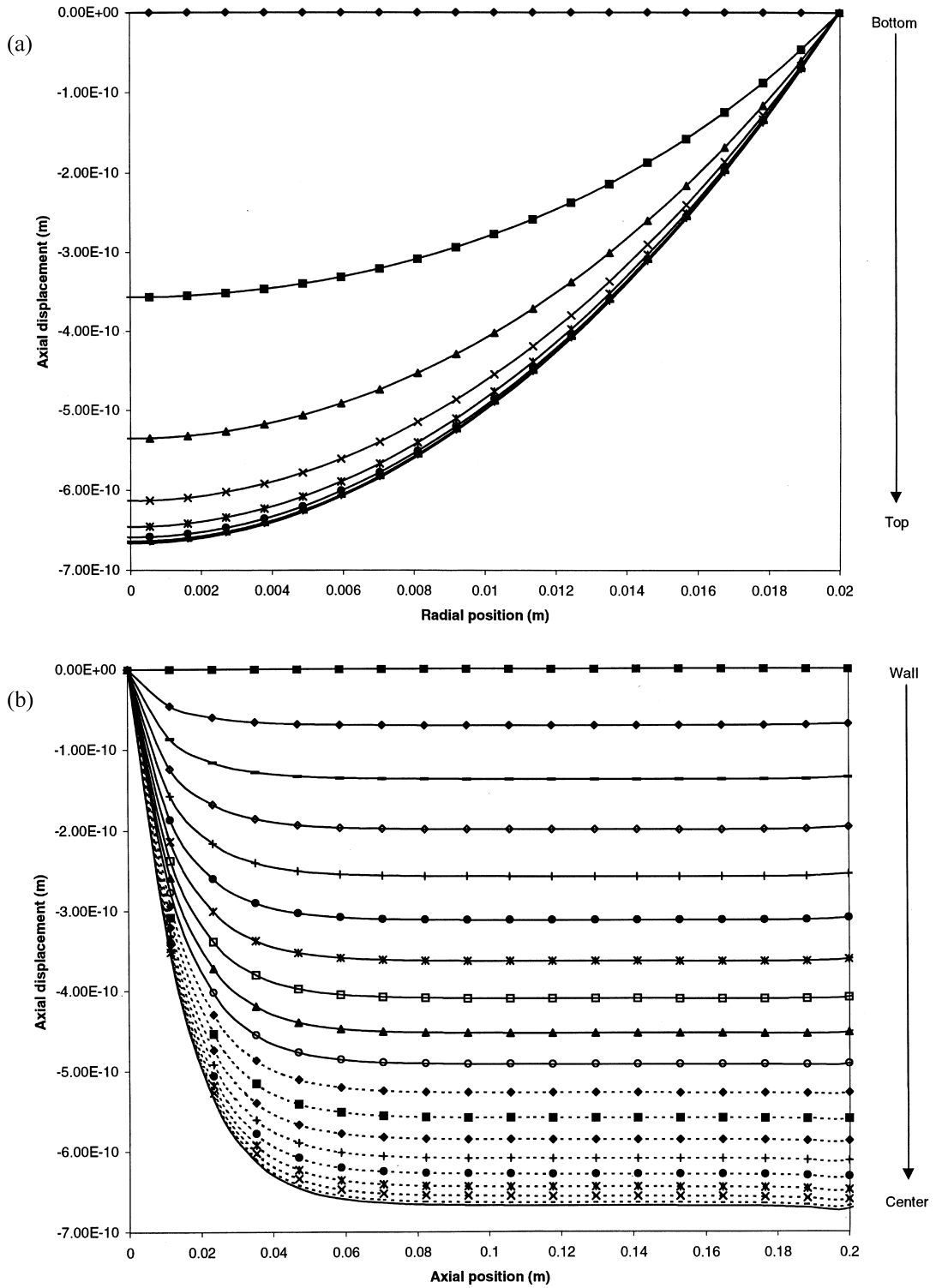

Fig. 1. Axial displacement result for a column of 0.04 m in diameter and 0.2 m in length ($L/D=5$): (a) displacement vs. radius, with the different lines corresponding to results at different axial positions; (b) displacement vs. column length, with the different lines corresponding to results at different radial positions.

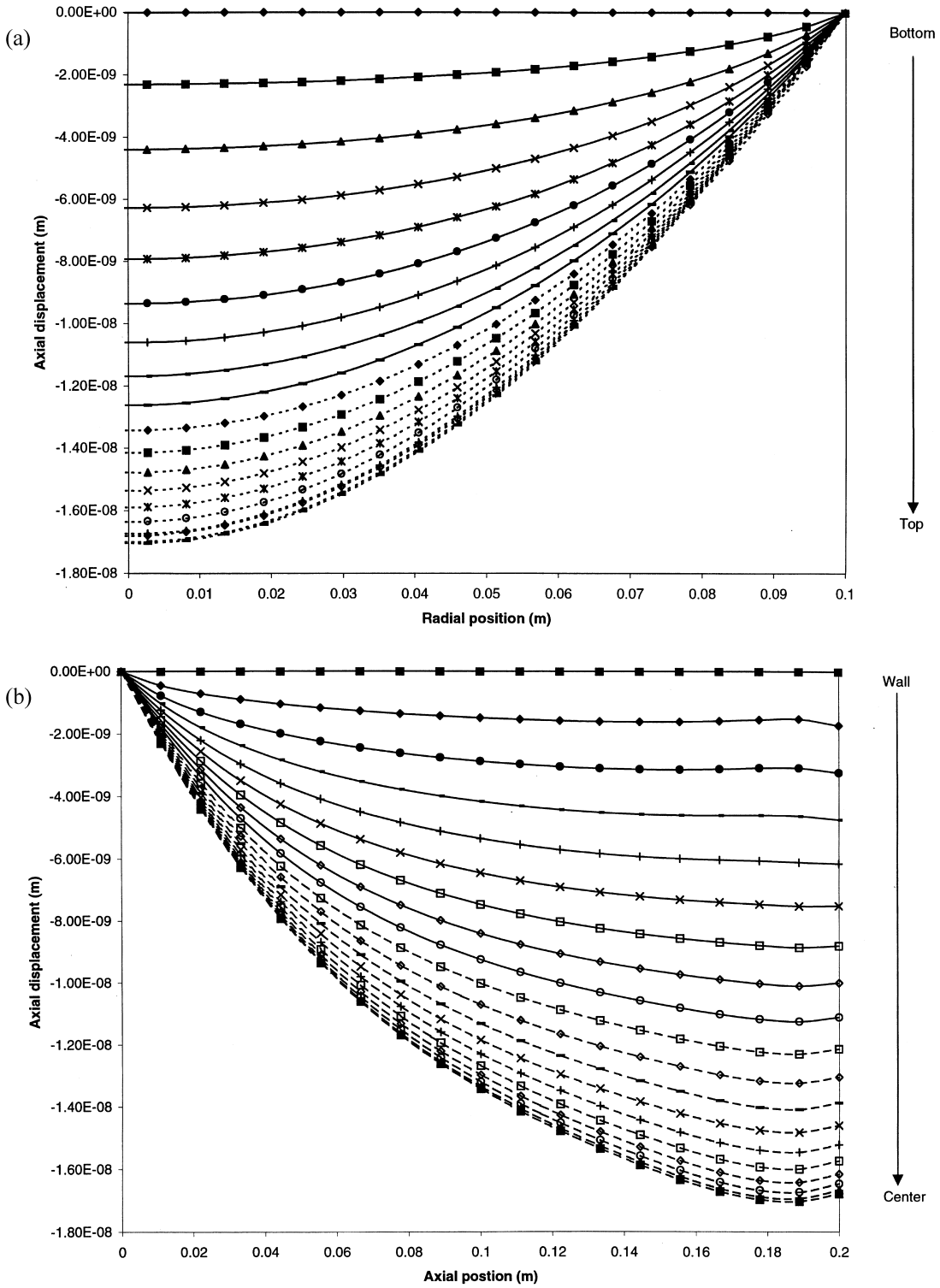

Fig. 2. Axial displacement result for a column of 0.2 m in diameter and 0.2 m in length ($L/D=1$): (a) displacement vs. radius; (b) displacement vs. column length.

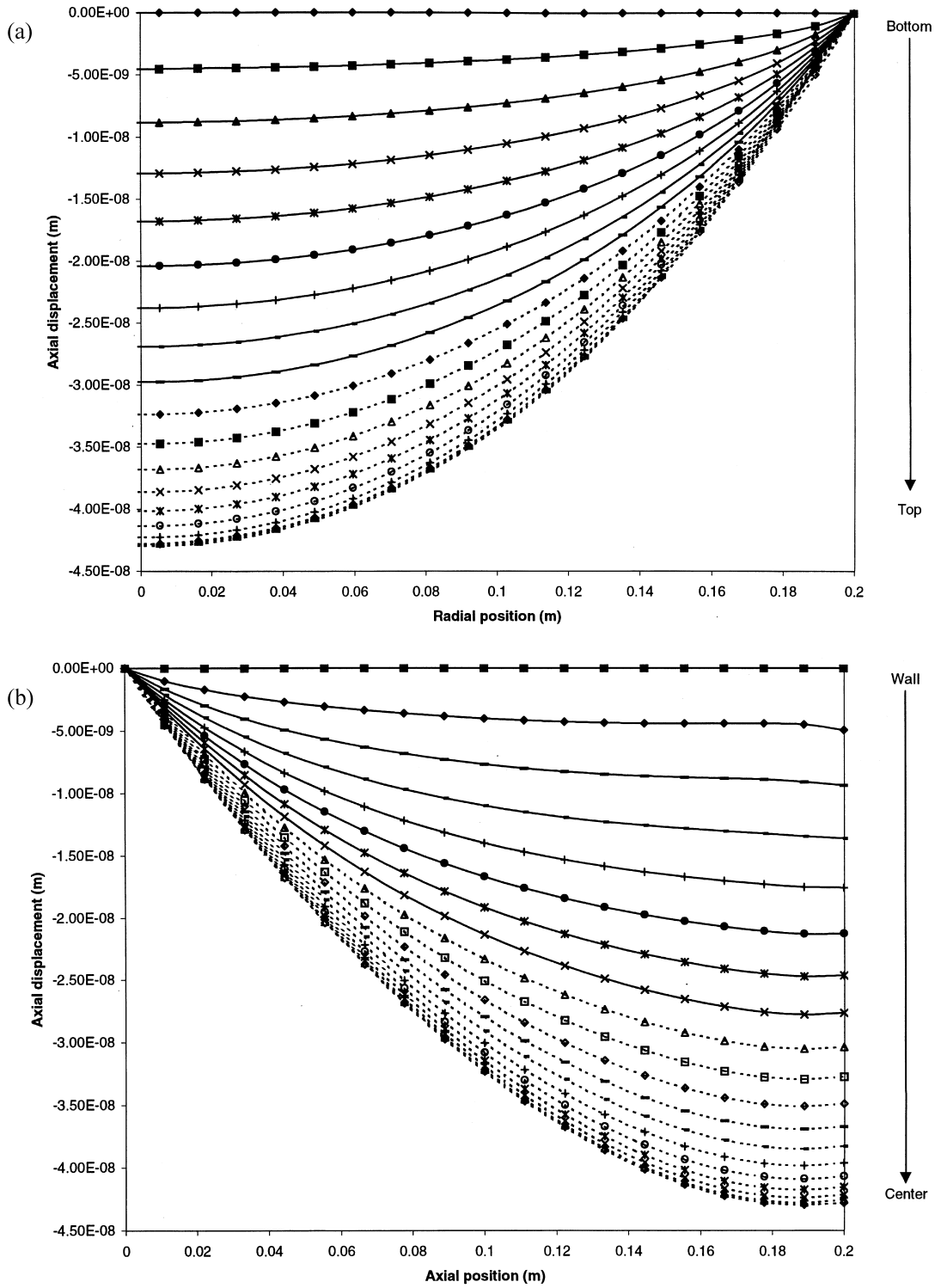

Fig. 3. Axial displacement result for a column of 0.4 m in diameter and 0.2 m in length ($L/D=0.5$): (a) displacement vs. radius; (b) displacement vs. column length.

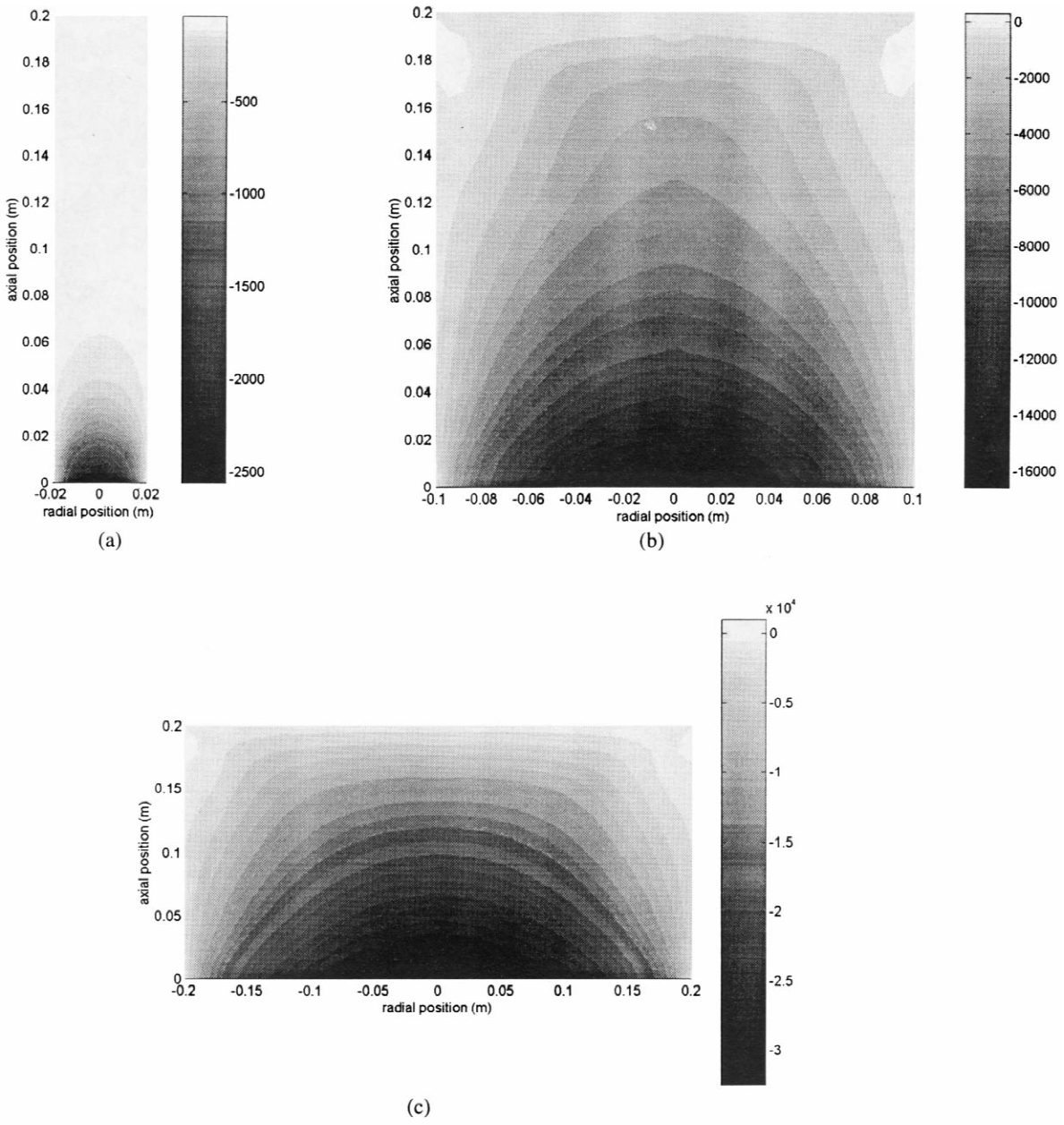

Fig. 4. Axial normal stress (σ_{zz}) results for the three columns simulated: (a) $L/D=5$; (b) $L/D=1$; (c) $L/D=0.5$.

gradients using Eq. (2), and the streamlines can be constructed and their residence times computed. The results of this analysis can be used to evaluate the header performance according to the two criteria listed above. Conventional distributors with a void space at column inlet are first analyzed, and the results show that such sudden expansions cause severe flow non-uniformity at the inlet of the packed bed.

To improve the current distributors, we investi-

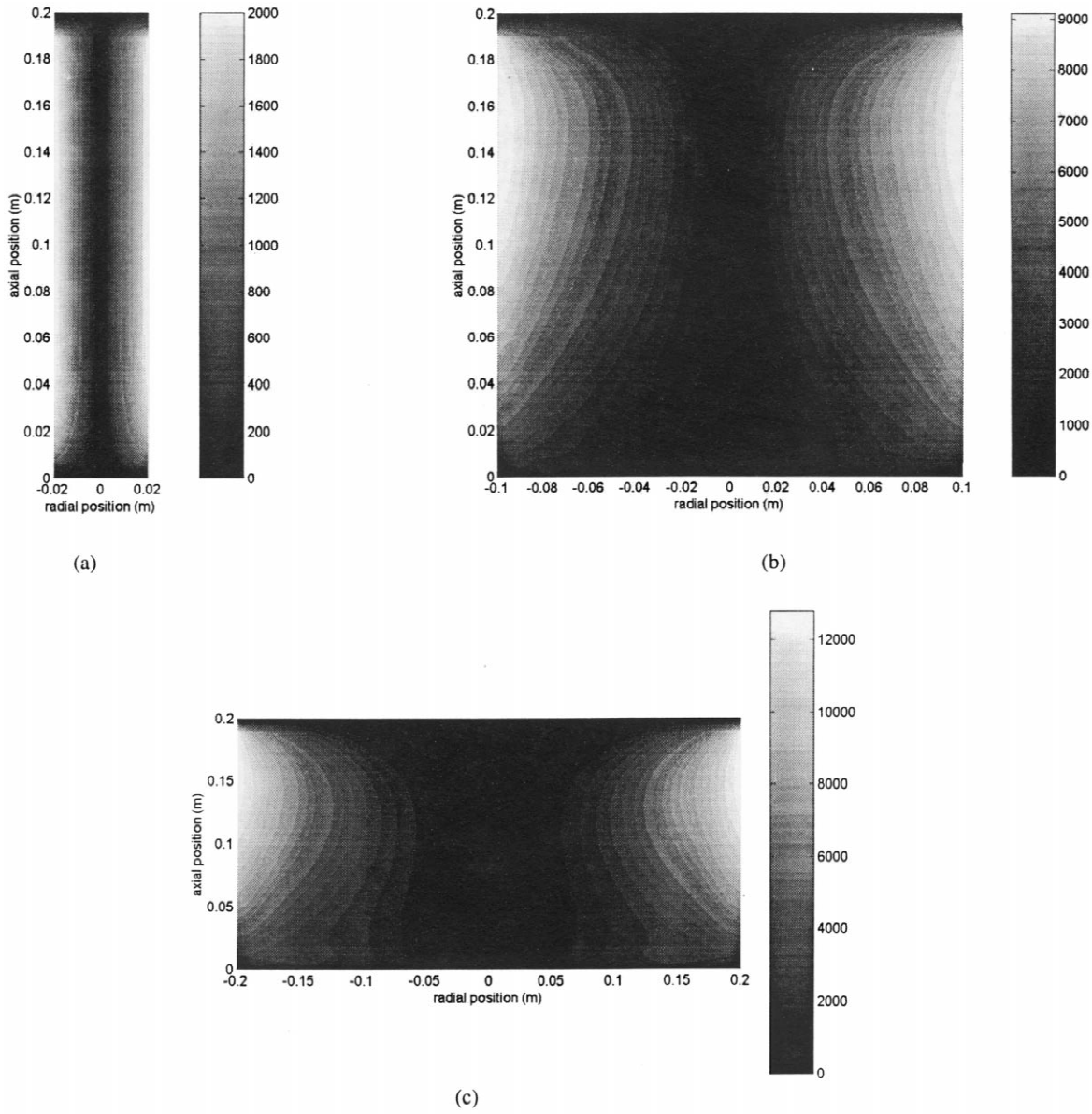

Fig. 5. Shear stress (σ_{rz}) results for the three columns simulated: (a) $L/D=5$; (b) $L/D=1$; (c) $L/D=0.5$.

gated a family of designs, illustrated by examples in Figs. 7 and 8, and to our knowledge it is a novel set of configurations. Headers in this group consist primarily of two regions, labeled collimator and manifold in the figures, both of which are constructed so that the fluid within them follows the laws of potential flow. A simple way of achieving this is to use porous solids such as sintered polymeric, metallic or ceramic particles, in which the pores or other flow channels are small compared to dimensions of the two regions.

The collimator section, which progressively thins with increase in radial position, contains primarily axial flow, whereas the manifold section serves to

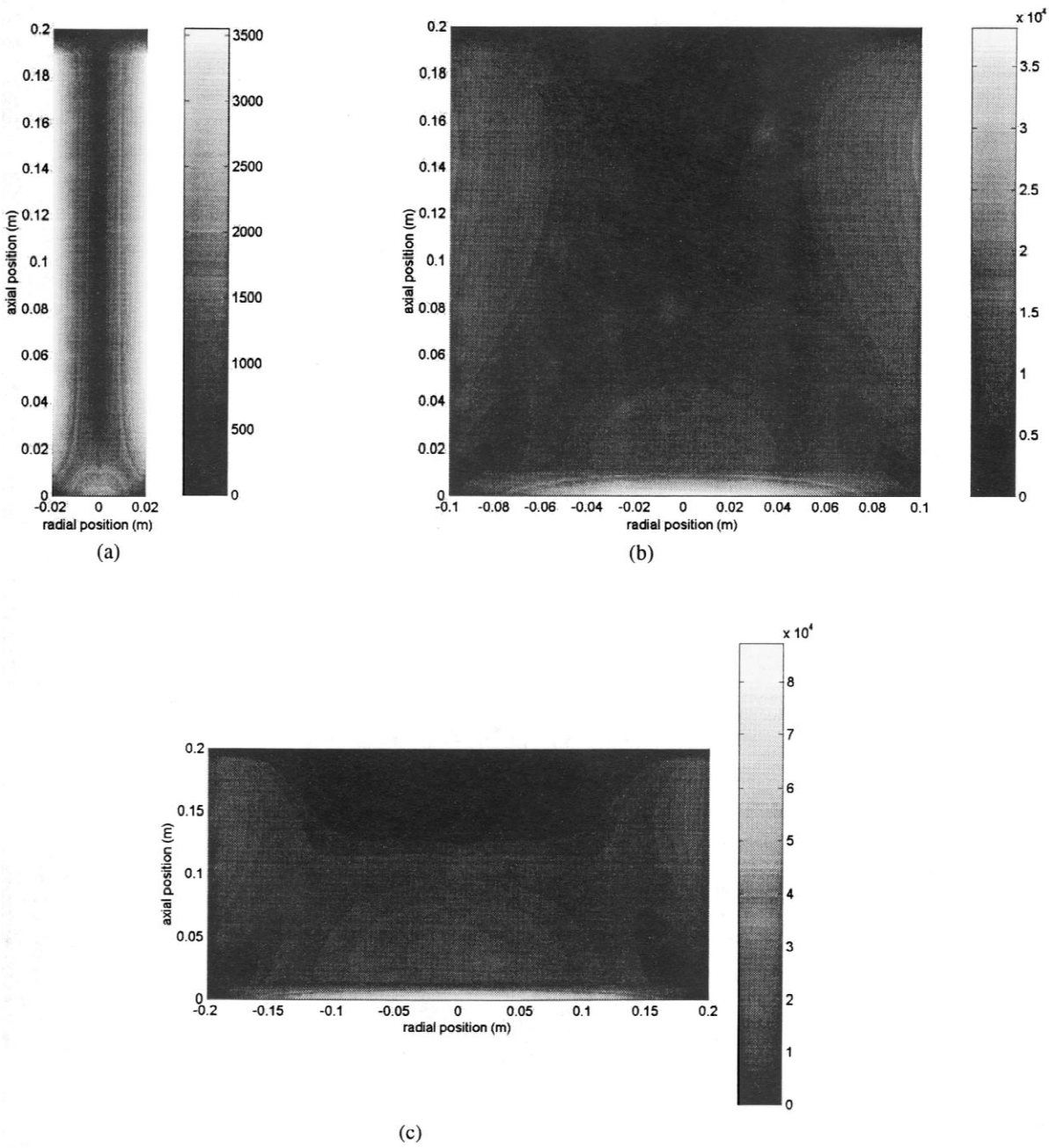

Fig. 6. Combined stress according to von Mises yield criterion for the three columns simulated: (a) $L/D=5$; (b) $L/D=1$; (c) $L/D=0.5$.

distribute fluid radially, and therefore contains mostly radial flow. The flow resistance per unit length in the direction of flow is greater for collimator than for manifold so that fluid moving directly down near the centerline takes more time to traverse the collimator than that at the periphery, and the radial flow in manifold permits fluid to move quickly towards the periphery to make up for its longer journey. A third

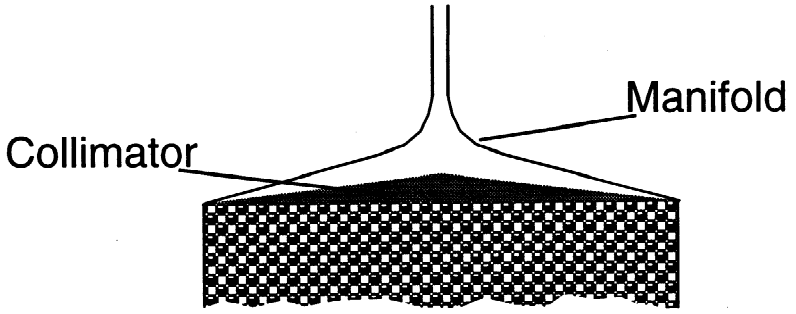

Fig. 7. Schematics of a non-flat header with a hyperbolic-shaped manifold.

zone, a mediator zone of uniform thickness and porosity can be added to protect the header against minor perturbations in the immediately adjacent packing. The following mathematical analysis show that such a distributor can be configured to achieve the desired uniform velocity profile as well as uniform hold-up time for all fluid elements.

3.1.1. Example 1

Consider as distributor a very squat cone such that its maximum height δ_0 is much less than its radius R (Fig. 7). Then flow through collimator can be considered to be axial, and the flow in manifold can be considered to be radial. In both regions, diameters of the particles comprising the two regions are very small relative to δ_0 and R. Under these conditions, Eq. (2) for each region simplifies to:

$$v_1 = -v_{1z} = \kappa_1 \cdot \frac{dP}{dz}; \quad \text{and} \quad v_2 = v_2 r = -\kappa_2 \cdot \frac{dP}{dr} \tag{15}$$

where v_1, v_2, κ_1 and κ_2 are velocities and permeabilities in the collimator and manifold regions, respectively. These are the equations for potential flow [18].

We now seek conditions such that at $z=0$, and all $0<r<R$, $v_1=v_0=$a constant; at $z=\delta(r)$, $P_1(r)=P_2(r)=P(r)$; and residence time on all streamlines are equal at $T=\delta_0/v_0$. Here v_1, v_0, $\delta(r)$ is the height of the region, and subscripts 1 and 2 indicate values in the collimator and manifold regions, respectively.

3.1.1.1. Region 1: the collimator

We begin by defining the behavior of the collimator which is fixed by the geometry chosen as:

$$\delta(r) = \delta_0(1 - r/R) \tag{16}$$

where δ_0 is the thickness at the axis. The pressure along the bounding surface between collimator and manifold is

$$P(r) = (v_0/\kappa_1)\delta(r) \tag{17}$$

The transit time through this region is

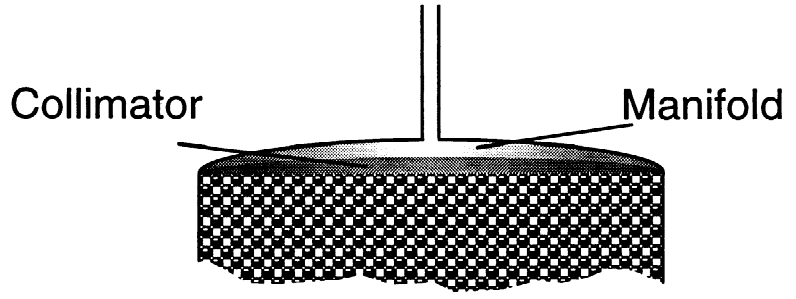

Fig. 8. Schematics of a non-flat header with a parabolic-shaped manifold.

$$t_1(r) = \frac{\delta(r)}{v_0} = \frac{\delta_0}{v_0}\left(1 - \frac{r}{R}\right) \tag{18}$$

and

$$\frac{dt_1}{dr} = -\frac{\delta_0}{Rv_0} = \text{constant} \tag{19}$$

Finally, the flow leaving the base of the collimator is

$$Q_1 = \pi r^2 v_0 \tag{20}$$

which completes our characterization of the collimator.

3.1.1.2. Region 2: the manifold

We now calculate the shape and porosity required in manifold region to meet our stated goals. The tangential flow in this region is

$$Q_2 = 2\pi rhv_2 = \pi R^2\left[1 - \left(\frac{r}{R}\right)^2\right]v_0 \tag{21}$$

where h is the height of this region. The second equal sign comes from the fact that the r-directional flow in the manifold must be equal to the total flow less the flow entering the collimator (Q_1). Thus

$$v_2 = \frac{R^2 v_0[1-(r/R)^2]}{2rh} \tag{22}$$

and

$$\frac{dt_2}{dr} = \frac{1}{v_2} = \frac{2rh}{R^2 v_0[1-(r/R)^2]} \tag{23}$$

Since $t_1 + t_2 = T$, it follows that $dt_2/dr = -dt_1/dr$, and

$$\frac{h}{\delta_0} = \frac{1}{2}\left[\frac{R}{r} - \frac{r}{R}\right] \tag{24}$$

which is independent of porosity. It follows from this result that

$$v_2 = v_0(R/\delta_0) = \text{constant} \tag{25}$$

Combining Eqs. (15) and (25) yields:

$$\frac{\kappa_2}{\kappa_1} = \left(\frac{R}{\delta_0}\right)^2 \tag{26}$$

which is the result we seek.

In this example, we have succeeded in obtaining a suitable header description, with the one ambiguity of a singularity at the system axis. However, this region is masked by the inlet tube itself. In practice, one need only maintain the calculated height outward from the feed tube radius. Further more, this design is simple, requiring only the machining of the two solids comprising collimator and manifold, and employing appropriate pore sizes in each.

3.1.2. Example 2

Here we consider changing the shape of the collimator section to

$$\delta = \delta_0\left[1 - \left(\frac{r}{R}\right)^2\right] \tag{27}$$

We can follow the development of example 1 and the height of the manifold is

$$h = \delta_0\left[1 - \left(\frac{r}{R}\right)^2\right] \tag{28}$$

Then if the collimator permeability is constant, we find that

$$\frac{\kappa_2}{\kappa_1} = \left[\frac{R^2}{2r\delta_0}\right]^2 \tag{29}$$

Infinite permeability at the axis can be approximated by free space. This header is shown in Fig. 8.

In both of these examples, the permeability of the collimator is considered constant. We can also use a collimator with radially varying permeability. A wide variety of designs is possible; since there are at least four variable parameters [$\kappa_1(r)$, $\kappa_2(r)$, $\delta(r)$, $h(r)$], and only two design goals (constant flow and constant residence time over radius), the fluid flow problem is underspecified and remaining parameters may be chosen for convenience.

3.2. Results and discussion

Numerical simulations of exiting velocity profile and residence time distribution are performed for both conventional distributor and improved designs, and the results are shown in Figs. 9–11. The radius (R) and δ_0 are kept constant in all three cases, where for the sudden expansion header, δ_0 is equal to the thickness of the frit. As seen in Fig. 9, while the sudden expansion header provides relatively uniform velocity profile at the exit, it fails to satisfy the

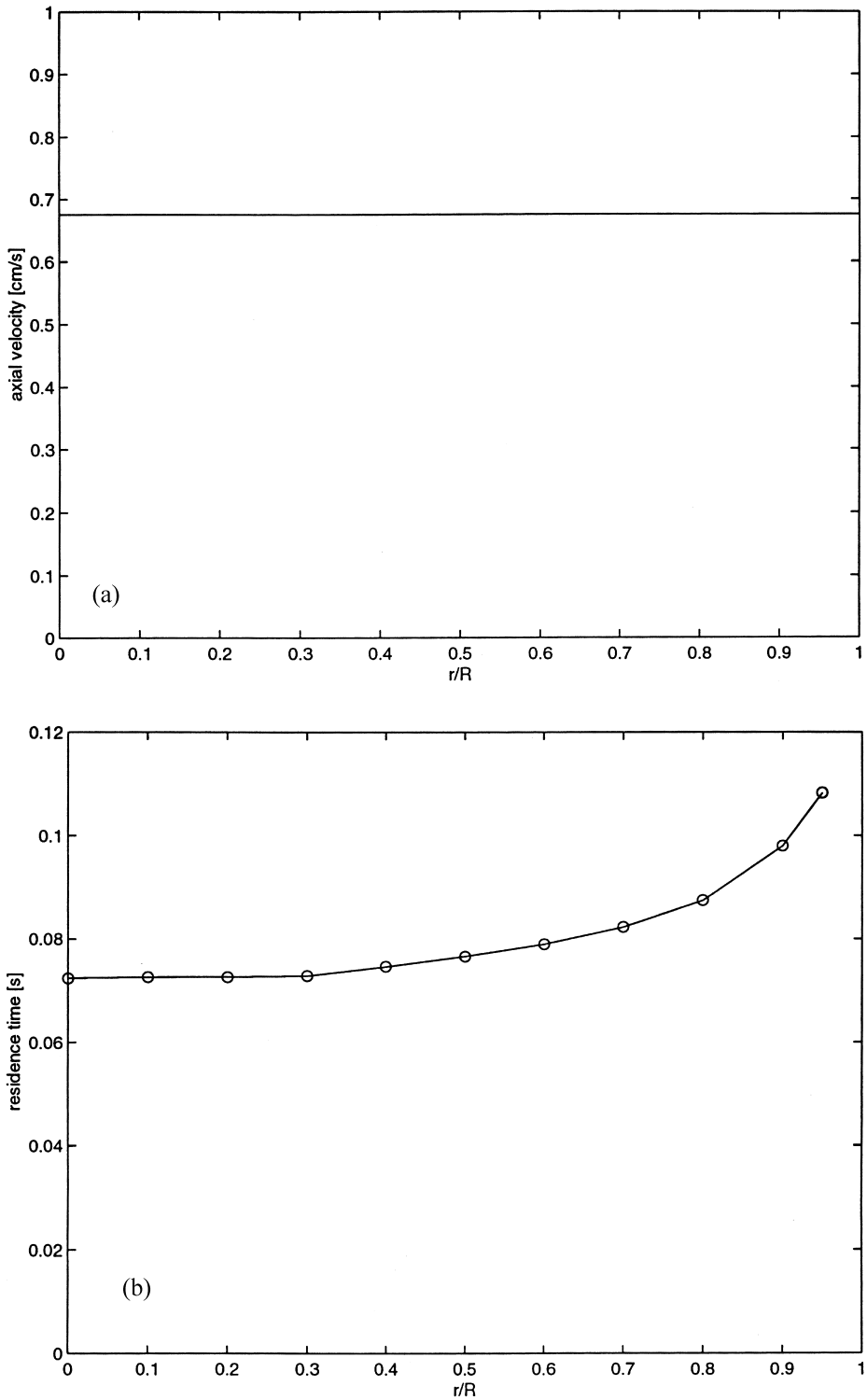

Fig. 9. Numerical evaluation results for a sudden expansion header: (a) axial velocity vs. radius; (b) residence time distribution in the radial direction. Both quantities are calculated at the exit of the header.

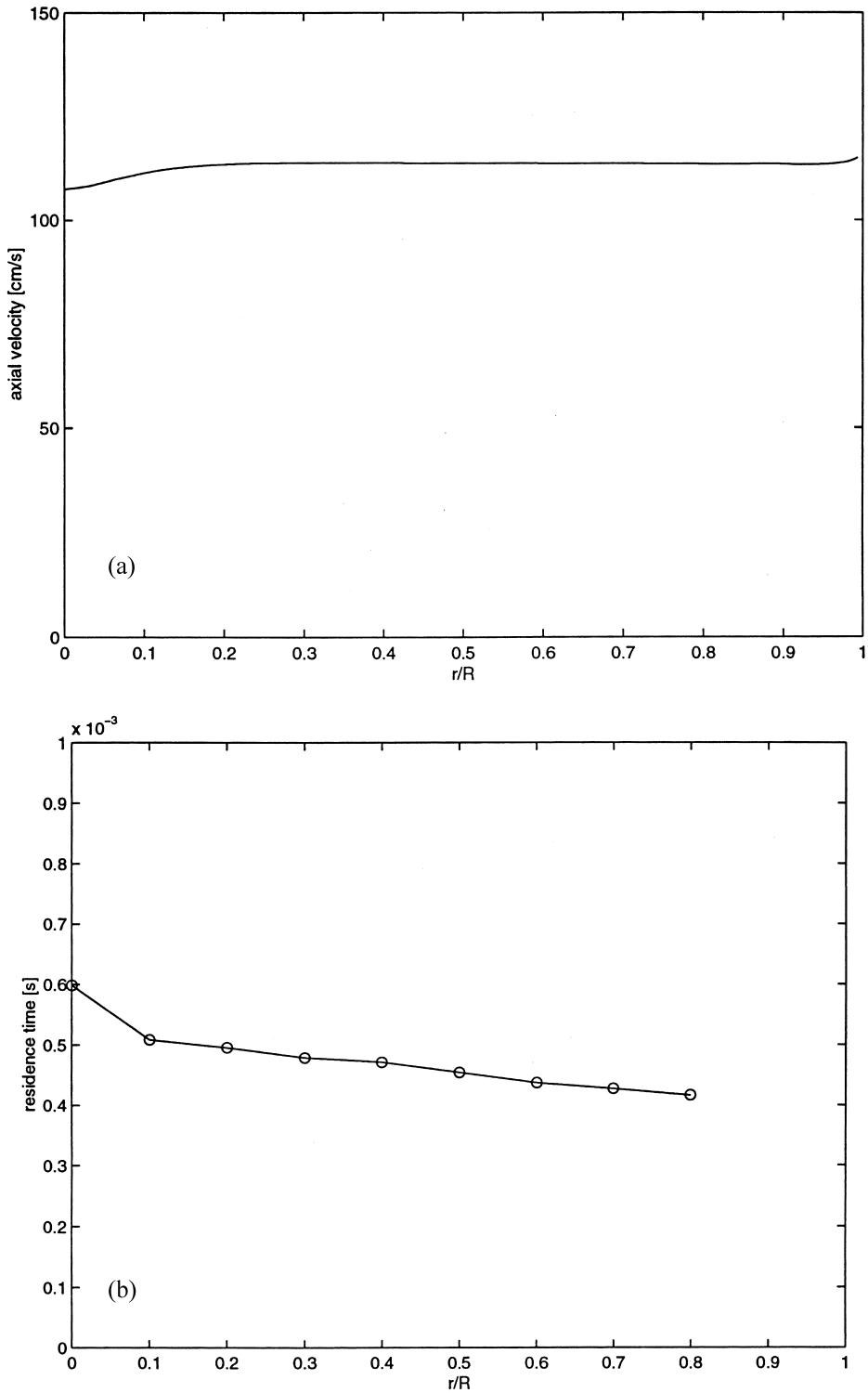

Fig. 10. Numerical evaluation results for a header sketched in Fig. 7: (a) axial velocity vs. radius; (b) residence time distribution in the radial direction. Both quantities are calculated at the exit of the header. The singularity in velocity near the wall is due to numerical errors.

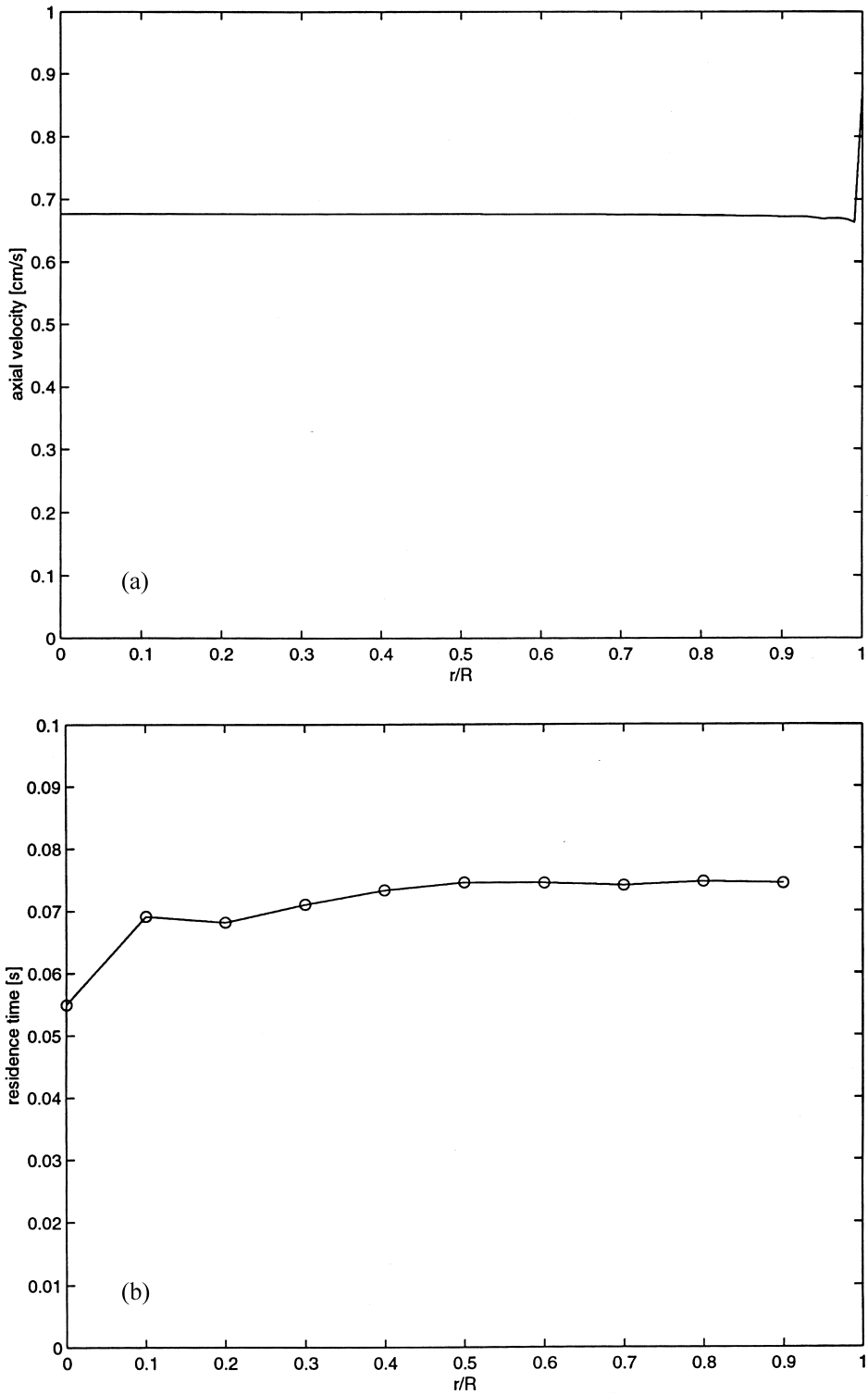

Fig. 11. Numerical evaluation results for a header sketched in Fig. 8: (a) axial velocity vs. radius; (b) residence time distribution in the radial direction. Both quantities are calculated at the exit of the header. The singularity in velocity near the wall is due to numerical errors.

residence time distribution criterion. The residence times of streamlines increase rapidly with radius due to the longer distances the fluid closer to the wall must travel. In Figs. 10 and 11, the velocity profiles and the residence time distributions for the two non-flat distributors are plotted. The sample header 1 (Figs. 7 and 10) does not conform to our expectations. This is because in the analysis above, a lubrication approximation based on a thin header is used. This approximation breaks down at some point as the thickness of the header increases towards the center. On the other hand, the sample header 2 (Figs. 8 and 11) shows a clear improvement from the sudden expansion header. The singular behavior of the velocities near the wall for both headers is caused by a numerical instability in the interpolation scheme.

The above results prove that a systematic approach can be followed to achieve better header designs. Neither of the sample headers shown here, however, has been optimized. The sample header 1 has the advantage of both regions having uniform porosity although the hyperbolic shape of the manifold could be undesirable. The sample header 2 has a nice parabolic shape, but the porosity of the manifold must vary in radial direction, which could be difficult to manufacture. Current efforts are focused on finding other optimal shapes for the header.

4. Conclusions

A model for description of the column packing process is being developed to explain the packing patterns observed in experiments. Stress distributions in elastic region suggest that the particles near the wall are subject to slipping sooner than those in the core region. Columns of different aspect ratios are examined and thinner columns have greater packing inhomogeneity. It can thus be concluded that in the elastic region, the most significant packing inhomogeneity for chromatography applications is caused only by wall effects.

A new approach to distributor evaluation based on fundamentals in fluid mechanics is developed and used to show the inadequacy of conventional headers. This approach also leads to a series of new designs which can provide substantially identical residence times and uniform exit velocities. The idea of developing a distributor which can correct other non-idealities such as packing inhomogeneity is raised. However, further studies must be done on the extent of column packing inhomogeneity and header capacity before this idea can be put to test.

References

[1] J.C. Giddings, J. Gas Chromatogr. 1 (1963) 12.
[2] J.H. Knox, G.R. Laird, P.A. Raven, J. Chromatogr. 122 (1976) 129.
[3] L.S. Eon, J. Chromatogr. 149 (1978) 29.
[4] J.E. Baur, E.W. Kristensen, R.M. Wightman, Anal. Chem. 60 (1988) 2334.
[5] T. Farkas, M.J. Sepaniak, G. Guiochon, J. Chromatogr. A 740 (1996) 169.
[6] D.K. Roper, E.N. Lightfoot, J. Chromatogr. A 702 (1995) 69.
[7] E.J. Fernandez, C.A. Grotegut, G.W. Braun, K.J. Kirshner, J.R. Staudaher, M.L. Dickson, V.L. Fernandez, Phys. Fluids 7 (1995) 468.
[8] A.M. Athalye, Ph.D. Thesis, University of Wisconsin-Madison, Madison, 1993.
[9] E. Bayer, W. Muller, M. Ilg, K. Albert, Angew. Chem., Intl. Ed. Engl. 28 (1989) 1029.
[10] U. Tallarek, E. Bauneister, K. Albert, E. Bayer, G. Guiochon, J. Chromatogr. A 696 (1995) 1.
[11] E. Bayer, E. Baumeister, U. Tallarek, K. Albert, G. Guiochon, J. Chromatogr. A 704 (1995) 37.
[12] J.H. Knox, J.F. Parcher, Anal. Chem. 41 (1969) 1599.
[13] T. Farkas, J.Q. Chambers, G.A. Guiochon, J. Chromatogr. A 679 (1994) 231.
[14] T. Farkas, M.J. Sepaniak, G.A. Guiochon, J. Chromatogr. A 740 (1996) 169.
[15] T. Farkas, M.J. Sepaniak, G. Guiochon, AIChE J. 43 (1997) 1964.
[16] T. Farkas, G. Guiochon, Anal. Chem. 69 (1997) 5592.
[17] F.G. Lode, MS Thesis, University of Wisconsin-Madison, Madison, 1997.
[18] L.R. Snyder, J.J. Kirkland, Introduction to Modern Liquid Chromatography, Wiley, New York, 2nd ed., 1979.
[19] R.B. Bird, W.E. Stewart, E.N. Lightfoot, Transport Phenomena, Wiley, New York, 1960.
[20] G.J. Kynch, Trans. Faraday Soc. 48 (1952) 166.
[21] F.M. Auzerais, R. Jackson, W.B. Russel, W.F. Murphy, J. Fluid Mech. 221 (1990) 613.
[22] C. Shen, W.B. Russel, F.M. Auzerais, AIChE J. 40 (1994) 1876.
[23] K.A. Landman, W.B. Russel, Phys. Fluids A 5 (1993) 550.
[24] B.J. Kellett, C.Y. Lin, J. Am. Ceram. Soc. 80 (1997) 381.
[25] H.K. Rhee, R. Aris, N.R. Amundson, First-Order Partial Differential Equations, Vol. I, Theory and Application of Single Equations, Prentice Hall, Eaglewood Cliffs, NJ, 1976, pp. 350–360.

[26] K.C.E. Östergren, A.C. Trägårdh, G.G. Enstad, J. Mosby, AIChE J. 44 (1998) 2.
[27] S. Kobayashi, S.I. Oh, T. Altan, Metal Forming and the Finite-Element Method, Oxford University Press, Oxford, 1989, Ch. 13.
[28] R.A. Thompson, Ceram. Bull. 60 (1981) 237.
[29] V. Saxena, P. Young, US Pat. No. 5 462 659 (1995).
[30] M. LePlang, D. Chabrol, US Pat. No. 5 141 635 (1992).
[31] R.J. McNeil, US Pat. No. 4 354 932 (1982).
[32] A.E. Colvin, Jr., M.W. Hanley, US Pat. No. 4 894 152 (1990).
[33] M.M. Kearney, K.R. Petersen, T. Vervloet, M.W. Mumm, US Pat. No. 5 354 460 (1994).
[34] T. Joseph, A.J. Pearson, R.C. Adams, O.A. Swift, US Pat. No. 5 324 426 (1994).
[35] A. Jungbauer, H.P. Letter, US Pat. No. 5 423 982 (1995).
[36] L.H. Mott, US Pat. No. 4 399 032 (1983).
[37] M.N. Munk, US Pat. No. 4 457 846 (1984).
[38] V. Saxena, B.D. Andresen, US Pat. No. 4 865 729 (1989).